Mechanics of Advanced Materials and Structures ›

Volume 31, 2024 - Issue 27

Full access

700 Views | 33 CrossRef citations to date | 4 Altmetric

Original Articles

Perforated auxetic honeycomb booster with reentrant chirality: A new design for high-efficiency piezoelectric energy harvesting

Mohammad Ravanbod & Salman Ebrahimi-Nejad

Pages 9857-9872 | Received 22 Aug 2023, Accepted 05 Nov 2023, Published online: 19 Nov 2023

Cite this article https://doi.org/10.1080/15376494.2023.2280997 Check for updates

Abstract

The present study develops an auxetic meta-structure booster to advance piezoelectric energy harvesting (PEH). The model comprised a three-dimensional (3D) cantilever beam equipped with an auxetic substrate bonded to a piezoelectric (PZT) point defect using an epoxy layer. The substrate used in this proposed energy harvester possesses an auxetic region responsible for generating auxetic behavior and concentrating stress in the PZT layer. The auxetic model called auxetic structure (AS)-II is inspired by ancient motifs and is designed based on the combination of several promising mechanisms, including reentrant, chiral, perforation, and honeycomb supercell. The finite element method is employed to create numerical models whose accuracy is confirmed by mesh convergence and available experimental data. A parametric study is conducted on the AS-II harvester to examine the influence of geometry and PZT material type on the harvested electrical power. Our research efforts stem fr… both mechanical and electrical circuit fields to fulfill the broadband design target within the desired ultra-low-frequency range of $1–20$ Hz, regardless of the resonance condition. As a result, the impact of other factors, such

investigated. The reason behind such outstanding performance of AS-II is explained in terms of geometrical physics and stress distribution. The effect of geometrical dimensions on the auxetic behavior is also analyzed using Poisson's ratio (PR) study. Subsequently, we demonstrate that this innovative adapter can advance the system's performance in terms of harvested power and lightweight by a magnification factor of 14.61 and 5.8 times that of a plain substrate and 2.25 and 3.16 times that of a conventional auxetic harvester, respectively. The present harvester is strain controllable, where it can set PR between -2 and 0, resulting in robust PEH even if switching input vibration from high to low levels. This new idea enables us to serve cantilever-type resonators at frequencies far lower than their resonant frequencies with small portions of incident excitement.

Keywords:

Auxetic metamaterial | negative Poisson ratio | vibration energy harvesting | piezoelectric | renewable energy | reentrant | honeycomb | chiral | ultra-low frequency

Previous article | **View** issue table of contents | **Next** article

1. Introduction

Vibration energy harvesting (VEH) techniques have been gaining significant attention in recent years due to their wide range of applications, from large-scale systems to micro and nano-scale applications. Vibration energy is a ubiquitous source of energy among ambient ones. It possesses the capability to be straightforwardly harvested and has embraced many scientists. Harvesting energy from ambient vibrations in various environments is an active line of research. This technology has tremendous promising applications, including supplying self-powered sensors in a wireless network like the Internet of Things (IoT), enabling battery-free monitoring systems, and cutting down on energy expenses associated with smart maintenance and structural health monitoring. Therefore, VEH is essential for self-powered systems as it offers a viable and cost-effective alternative to batteries. Moreover, this approach contributes to reducing greenhouse gas emissions and preserving the environment. Three commonly used methods for converting vibration energy into electricity are triboelectric [1, 2], electromagnetic [3, 4], and piezoelectric (PZT) [5–7]. PZT transduction is highly valued for its outstanding power density and easy integration into small-scale energy harvesting systems [8]. The VEH has made substantial use of PZT elements, where a mechanical force applied on the PZT layer can be directly converted to reliable electrical energy. Nevertheless, the main obstacle remains the low power and efficiency of the PZT-based energy harvesters. To overcome these limitations, advancements are made in material science by altering the composition of PZT elements [9] or concerning structural solutions such as utilizing metamaterials [10].

Mechanical/acoustic metamaterials [11] belong to a class of synthetic materials that can be artificially manufactured and adjusted to control and suppress the propagation of mechanical/acoustic waves due to their abnormal characteristics called "bandgaps" (BG). The unique characteristics of metamaterials make them versatile for a variety of applications, such as vibration control [12], sound attenuation [13, 14] and VEH [15]. Various types of metamaterials are available, including perforated [16], reentrant [17], convex scatterer [18], cavity [19], honeycombs [20], chiral [21], Kirigami [22] multi-resonance systems [23], Helmholtz mechanism [24], and membrane types [25]. Metamaterials can be classified into two main types: Bragg scattering [26] with wide bandgaps in the relatively high-frequency range, and local resonant metamaterials (LRM) [27], which generate

The emergence of mechanical and acoustics metamaterials has introduced a reliable method to enhance piezoelectric energy harvesting (PEH) among conventional mechanisms such as cantilever beams. Ma et al. [28] proposed cavity-based metamaterials that improve the PEH performance at the local resonance frequency of around $15\ \mathrm{KHz}$. In an effort to enhance PEH, Sun et al. [29] adjusted the resonance frequency and geometry parameters of a metamaterial plate substrate. They were successful in creating a metamaterial booster that was able to extract a maximum power of $195.52\ \mu\mathrm{W}$ at $1329\mathrm{Hz}$, with a substrate size of $90\ \mathrm{mm}$ and a side PZT plate of $30\ \mathrm{mm}$, using an input sound pressure of $49.2\ \mathrm{Pa}$. Askari et al. [30] developed a multi-beam piezo-based metamaterial harvester capable of generating milliwatts powers under a harmonic base acceleration of 0.4 g, where the harvester has a resonance frequency of less than 100 Hz.

Zhao et al. [31] considered a graded metamaterial energy harvester that integrates the PEH operation for low-frequency ambient vibrations. Wu et al. [32] created a honeycomb metamaterial using the quantum valley Hall impact, and by disrupting the symmetry of the crystal, a substantial BG is formed. Also, a topological interface is established between two crystal phases that is evaluated for its ability to withstand defects and disorders. The forged robust and condensed topological edge state is then utilized to design an energy harvester with superior performance in both vibration insulation and PEH. Raghavan et al. [33] reported an LRM structure composed of ionic polymer metal composites (IPMC) for improving PEH performance by tuning resonance frequency. Through numerical analysis, the LRM energy harvester's defect mode and key parameters that can generate the highest voltage are determined. Rezaei et al. [34] introduced a new approach to PEH for acoustic waves in quarter-wavelength tubes by incorporating a nonlinear restorative load into the PZT patch of an acoustic cantilever beam. This manipulation extended the resonance bandwidth and improved the overall PEH performance.

Previous studies have indicated that inertial harvesters rely on a specific resonant frequency for optimal power output. If the frequency falls outside this range, the amount of power generated will significantly decrease. It is worth noting that the resonance frequency tends to exceed $200\ Hz$. Alternatively, the use of auxetic materials in the harvester enables strain energy harvesting without depending on the harvester's resonant condition. This approach can help to minimize the negative strain impact on the host structure [35] while maximizing the extracted strain energy [36]. Auxetic materials and structures [37, 38] are a class of metamaterials with negative Poisson's ratio (NPR) properties, meaning they expand sideways when subjected to tension or contract laterally under compression. In engineering applications, auxetic sandwich structures have shown the potential to improve shock and impact saturation [39], shear resistance [40], bending stiffness and fracture toughness [41], energy absorption [42], and vibro-acoustics performance [43]. Research into using the auxetic feature for energy harvesting is a new area of exploration, starting in 2017 [44]. To name a few works; Eghbali et al. [45] studied two distinct circular auxetic designs mounted on the conventional cantilever beam. The result showed that the auxetic models would reach 10.2 and 13.3 magnification factors at the resonance frequency compared to the PZT plain harvester. Zhu et al. [46] theoretically investigated the impact of variations in geometry parameters on the mode frequency and energy response of a honeycomb auxetic sandwich plain. Sadikbasha [47] proposed an auxetic hexachiral cantilever beam for the PEH enhancement at a low-frequency range. Their harvester had a natural frequency of $23\ \mathrm{Hz}$ and an extracted voltage of $9.1\ \mathrm{V}$ at $250\ \mathrm{k}\Omega$. Chen et al. [48] designed a nonlinear PZT energy harvester using a clamp-clamp beam substrate with a reentrant hexagonal auxetic booster, resulting in higher bandwidth and PEH rate. Ferguson et al. [49] developed an auxetic cantilever structure for improving the PEH performance of the PZT layer. The results showed that under a $250\ \mu\mathrm{W}$ peak-to-peak sinusoidal strain at $10\ \mathrm{Hz}$,

et al. [50] considered a plucking rotational piezoelectric-magnetic-based harvester with an auxetic structure, which improves rotational energy harvesting power output under low frequencies using frequency up-conversion and auxetic mechanisms. Chandha et al. [51] analyzed a lightweight bimorph beam consisting of multifunctional magneto-electro-elastic (MEE) plains and auxetic structure core for improving PEH performance. The harvested power of the proposed auxetic-based harvester was nearly 1.5 times greater than that of the conventional metal-based harvesters, while the weight of the system was reduced by 22%. Fathi et al. [52] employed an auxetic design to enhance the PEH performance of a sandwich beam harvester. The result showed a $30\,\%$ improvement in power output at $50\ \mathrm{Hz}$.

Over the years, several beam theories have been developed to study the behavior of beam structures, including classical beam models based on Euler-Bernoulli beam theory (EBBT) and Timoshenko beam theory (TBT). While classical beam models give satisfactory results for slender structures, they are less accurate for multi-layered, thin-walled, and open-section beams [53]. Higher-order shear deformation beam theories (HSDT) have been proposed to overcome the limitations of classical beam modeling, but they could not accurately account for warping and bending/torsion coupling. Ultimately, Carrera Unified Formulation (CUF), a refined theory, can capture non-classical effects and consider the effect of normal deformation, providing more accurate and efficient results in the vibration analysis of beams, plates, and shells [54, 55]. The CUF has been widely employed for many vibration analyses in mechanical, civil, and aerospace engineering structures. Filippi et al. [56] calculated the mechanical properties of kinematic one-dimensional and two-dimensional (1D) and (2D) beams and shells finite elements utilizing CUF. He et al. [57] utilized CUF to compute the vibration responses of a functionally graded cylindrical beam under thermal conditions. Shen et al. [58] developed a higher-ordered beam finite element using CUF to detect damage study of a newly reinforced beam. The finite element method (FEM) is a commonly used analysis method to calculate the vibration responses, including resonance frequency, stress distributions, and deformations under different excitements. However, in complex multi-dimensional systems, the numerical simulations might be extraordinarily complex with employing high-order mesh sizes, resulting in high-volume computations and time consumption. As a result, CUF can be an alternative solution to deal with such computational costs.

According to the literature, it is evident that PZT patches have a low-efficiency rate when it comes to extracting input energy at low frequencies, making the main challenge to their practical use. This consequential limitation restricts the utilization of such PZT patches to narrow lab applications. Indeed, it is impractical to extract the desired amount of energy in industrial applications unless the input vibration level is sufficiently high. A further critical concern is ensuring the system operates efficiently near the resonance frequency range, out of which the system's performance will inevitably plummet, causing the majority of incident energy waves to disappear. As an attempt to resolve the addressed problems, this paper proposes a novel piezo-cantilever beam strain energy harvester with a unique mechanical meta-structure inspired by ancient motifs to enhance PEH. The substrate used in this proposed energy harvester possesses an auxetic region responsible for generating auxetic behavior and concentrating stress in the PZT layer. Furthermore, the auxetic model is designed based on the combination of several promising mechanisms, including reentrant, chiral, perforation, and honeycomb supercell. Each of these mechanisms has already demonstrated its potential for PEH improvement. Subsequently, we demonstrate that this innovative adapter can advance the system's performance in terms of harvested power and lightweight by a magnification factor of 14.61 and 5.8 times, respectively, within the desired extremely low-frequency range of $1–20\ \mathrm{Hz}$, regardless of their resonance condition. The present harvester is strain controllable, where it can set PR

between -2 and 0, resulting in robust PEH even if switching input vibration from high to low levels. This novel idea allows us to serve cantilever-type resonators at frequencies far lower than their resonant frequencies.

Two different three-dimensional (3D) auxetic models are developed. Our research efforts stem from both mechanical and electrical circuit fields to achieve the broadband design target, utilizing the FEM whose accuracy is verified by available experimental data. As a result, the influence of geometry and material parameters on the PEH performance has been investigated, and the proposed model has been optimized in light of the outcomes. Also, stress levels and distribution in the PZT layer and substrate are studied to see how their changes influence the PEH rate. Meanwhile, the impact of shock magnitude, frequency, and bonding strength on the power output is studied. Eventually, the model's potential for improving maximum and average extracted power is analyzed, and the results are compared with the plain substrate. For the electrical circuit study, the impact of increasing load resistance on the PEH performance is further examined. The auxetic behavior of different models is examined by a PR analysis under the solid mechanic domain. The effect of changes in geometry parameters on the PR has been further studied to see how PR alteration with increasing a specific geometry size responds to the auxetic structure (AS)-II PEH performance. Finally, the project is wrapped up with a comparison of models based on their weight, considering the current industrial prevalent policy of employing lightweight structures. The proposed novel concept is applicable for self-power and wireless sensors in industry and IOT network environments where sensors consume the harvested renewable power to sense physical parameters. The wireless network also utilizes a portion of the power output to communicate and transfer signals.

2. Fundamental of piezoelectric energy harvesting

The PZT element can convert mechanical energy into electrical energy through direct PZT effects. We are utilizing this property to generate electric power from mechanical vibrations in a cantilever beam. To enhance the PZT performance, we propose using auxetic structures as boosters under the PZT patch. This mechanism will help concentrate stress and incident energy density in the PZT layer. Based on the PZT constitutive equations, we have the two primary equations presented below [59]:

$$D_3 = d_{31}\, T_1 + \varepsilon_{31}^{E}\, E_3 \tag{1}$$

$$S_1 = s_{11}^{E}\, T_1 + d_{31}\, E_3 \tag{2}$$

Where D_3 is the electric charge density; d_{31} denotes the PZT strain constant ($d_{31} = d_{32}$); ε_{31}^{E} denotes the dielectric constant under persistent stress; S_1 is the strain, s_{11}^{E} stands for the electric compliance in a constant electric field; and T_1 denotes the stress in the length direction of the PZT patch. It is observed that the electric charge density is directly proportional to the tensile stress. Due to the auxetic booster, the identical stress is concentrated into the PZT layer, resulting in a heightened electrical power density. In order to calculate electric power harvested, it is essential to determine the voltage output and optimal load resistor. Therefore, the open-circuit voltage output of the PZT patch operating under bending mode can be governed by:

$$V = \frac{t_p\,(d_{31}\overline{\sigma}_{11} + d_{32}\overline{\sigma}_{22})}{\varepsilon_{33}^{T}}$$

(3) where t_p and A_p are the thickness and area of the PZT layer; f denotes the excitation frequency; ε_{33} denotes the PZT relative permittivity; $\overline{\sigma}_{11}$ and $\overline{\sigma}_{22}$ stand for the average axial (*x*-axis) and lateral (*y*-axis) stresses in the PZT layer. Consequently, by connecting the PZT patch to an optimal load resistor R (Eq.4), the electric power will be generated.

$$R = \frac{t_p}{2\pi f \varepsilon_{33}^{T}\, A_p}$$

(4)

In addition, when a uniaxial strain is applied to the substrate at frequencies far below its resonance frequency, the PZT power output can be formulated as [60]:

$$P_{ext} = \frac{\left(\frac{V}{\sqrt{2}}\right)^2}{R} = \frac{\pi f\, t_p\, A_p\, d_{31}^2}{\varepsilon_{33}^{T}}\left(\overline{\sigma}_{11} + \overline{\sigma}_{22}\right)^2$$

(5)

It is suggested by Eq.(5) that the contributions of $\overline{\sigma}_{11}$ and $\overline{\sigma}_{22}$ to power extraction are equal. In general, conventional energy harvesters have positive PR for both the substrate and PZT layer, with similar values. The transverse contraction of PZT and substrate occurs uniformly during stretching, causing negligible external lateral force on the PZT. Also, the piezo's Poissonian contraction has principally increased $\overline{\sigma}_{22}$. This phenomenon sets lateral stress into an opposite sign and lower value than axial stress. As a result, the axial stress would dominate harvested power properties for conventional strain harvesters. On the other hand, in the case of the substrate with an NPR; the substrate undergoes lateral expansion when subjected to tension. Therefore, $\overline{\sigma}_{22}$ increases (and if the force is great enough, it will adopt the same sign as $\overline{\sigma}_{11}$). Consequently, $\overline{\sigma}_{11}$ and $\overline{\sigma}_{22}$ are able to equally provide contributions in power generating.

3. Fundamental of Poisson's ratio

Assuming that the structure only experiences the vertical load f_s along its top side while the lower side remains static. The lateral sides are subjected to free boundary conditions. As a result, based on the second Newton's law and isotropic linear solid mechanics, PR, the associated displacement, and strain equations under the frequency-domain can be derived in the following manner:

$$0 = \nabla . S + f_s$$

(6) where the deflection force responding is indicated by $\nabla . S$. The equations for the axial and lateral displacements can also be stated as follows applying Castigliano's second theorem: where E_s denotes the default material's Young's modulus, lx and ly are the practical cross-sectional length, A_x and A_y are the cross-sectional

areas, and δ_x and δ_y are displacements in the directions of x and y, respectively. Consequently, the induced strain and the tensile strain in the axial and lateral directions can be governed by:

$$\varepsilon_x = \frac{\delta_x}{lx} = \frac{\int_0^{lx} \frac{f_s}{E_s A_x}\, ds}{lx}$$

(7)

$$\varepsilon_y = \frac{\delta_y}{ly} = \frac{\int_0^{ly} \frac{f_s}{E_s A_y}\, ds}{ly}$$

(8)

Finally, the equivalent PR can be calculated by:

$$\upsilon_{xy} = -\frac{\varepsilon_y}{\varepsilon_x}$$

(9) where υ_{xy} shows the PR which describes the ratio of strain in the y direction to that in the loaded x direction.

4. Models and methods

Reentrant chiral auxetic structures (RCA) are types of auxetic designs that possess NPR properties within the range of -3 to nearly 0, unlike typical auxetic isotropic materials with NPR values that fall between -1 to almost 0 [61, 62]. Auxetic architectures of various types were previously explored and examined by scientists to enhance PZT performance. However, as a contribution, two auxetic structures named auxetic structure I (AS-I) and auxetic structure (AS-II) are used in this investigation, as depicted in Figure 1. AS-I demonstrated NPR properties and had already been used by many researchers for PEH applications [49, 61, 63], making it a promising candidate for our study verification. In the case of AS-II, multiple physics and mechanisms, including reentrant, chiral, honeycomb supercell, and rectangular and zigzag-shaped perforations, have been utilized to design a complex-based auxetic metamaterial structure that can exhibit NPR more than -1. AS-II is inspired by ancient motifs and is known as a reentrant chiral honeycomb auxetic metamaterial. AS—II consists of 4×4 unit cells periodically arranged among the x and y axes. The physics behind choosing such a structure can be explicated, in terms of four main factors. Because of the structural properties, the wave path has frequently changed, enabling the propagation of elastic waves to be circulating more inside the structure (see Figure 1(c) and Figure 2). As a result, there is a higher potential of waves being trapped and attenuated due to and reentrant zigzag network frames. The second reason is that the trapezoidal chirality connections concentrate the tension in the edges and side corners and transfer more elastic energy into the PZT layer. Consequently, this will improve PEH. The third reason is related to the utilization of the holey plate and rectangular perforations, which shifts the bands to lower frequency ranges and simultaneously reduces structure weight. Another reason is related to the use of honeycomb supercells by dividing the structure into some sub-unit cells. Many previous studies have verified that increasing the number of sub-cells would improve vibration control characteristics by increasing elastic wave absorption and transmission loss across a desired frequency range. We are interested in determining if it can be applied to PEH applications.

Figure 1. 2D view of the conventional plain and auxetic models.

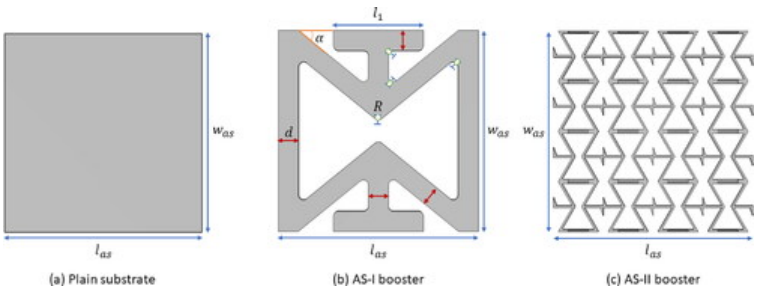

Display full size

Figure 2. Illustration of (a) the proposed auxetic unit-cell consisting of orthogonally arranged holes and (b) the periodic ordered auxetic super-cell comprising 4×4 unit-cells.

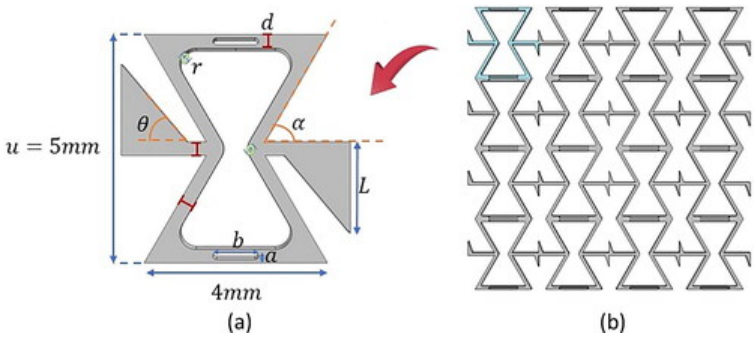

Display full size

The present work illustrates the schematic of both the conventional PZT beam and the proposed auxetic energy harvesters in Figure 3. The plan is to bond a PZT layer to a host plate equipped with an auxetic structure where the host is a cantilever beam with multiple potential applications as an energy converter. The reason behind utilizing such auxetic designs is that: the PZT elements can be stretched/or shrunk in two directions simultaneously by the auxetic domain, increasing extracted electric power. In addition, the auxetic area has a lower stiffness than the rest of the substrate, which results in a concentration of stress on the PZT patch. This phenomenon leads to an enhanced power density of the energy harvester based on the auxetic mechanism.

Figure 3. Schematic view of different system configurations for PEH.

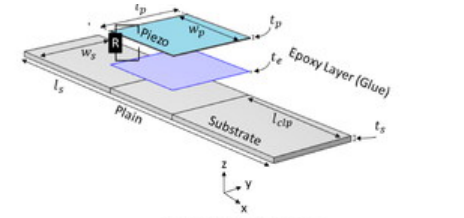

(a) Conventional model

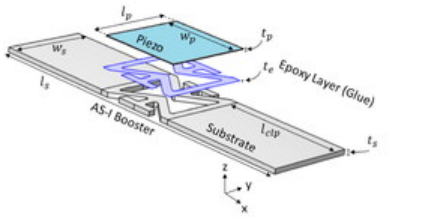

(b) PZT energy harvester equipped with AS-I booster

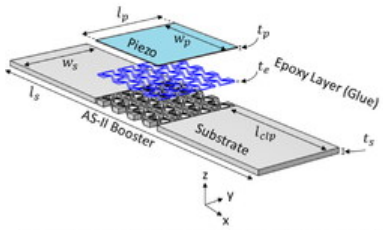

(c) PZT energy harvester equipped with the proposed AS-II booster.

Display full size

5. Finite element modeling

Under coupled mechanical and electric circuit fields, finite element (FE) modeling with COMSOL Multiphysics® 6.0 [64] is implemented to examine the effectiveness level of the presented auxetic booster in improving PEH performance. The developed FE models are schematically displayed in Figure 3 with an exploded view and in Figure 1 with an isolated auxetic area. In this research, the proposed model AS-II includes a steel substrate with a reentrant chiral honeycomb super-cell serving as its auxetic region. On top of this is a layer of PZT material known as PZT-5H, which belongs to the lead zirconate titanate class. Besides, an $8\ \mu m$ thick layer of epoxy is applied between the substrate and the PZT layer to bond them. Geometry sizes and material characteristics are listed in Tables 1 and 2, respectively. The provided values in the tables are the optimal ones, which are optimized in the following sections.

Table 1. Structural parameters used in the models.

Display Table

Table 2. Material properties used in the analyses.

Display Table

The substrate features two clamped sections of equal length of l_{clp} located at both ends. One is fixed in place, while the other is subjected to a body load with a magnitude of $0.9e^6\mathrm{N}/\mathrm{m}^3$ (for the low incident vibration study) and a $2.3e^6\mathrm{N}/\mathrm{m}^3$ body load that is 2.5 times or $61\,\%$ higher (for the high incident vibration study) in the z-direction at a frequency of 10 Hz on the free section of the substrate. To ascertain the highest possible harvested power, a load resistor is tied across the electrodes on the top and bottom faces of the PZT segment, whose load resistance is specified using Eq. (4) to match the internal impedance of the PZT layer.

The initial load resistance R = 378 $k\Omega$, and its value will be optimized in the following section. In addition, the thin elastic layer (TEL) is added at the epoxy's interfaces with the substrate and the PZT device to compensate for bonding defects. The TEL is a spring boundary condition (spring constant) provided within COMSOL representing the layer bonding strength that bonds the contacting faces entirely by visco-elastic forces proportional to their relative displacement and velocity. During the design stage, the estimated TEL value is initially set to $220\ \mathrm{GN}/\mathrm{m}^3$ [49], although it will ultimately be determined through sensitivity analysis.

An equivalent conventional plain energy harvester called "plain substrate" was also designed to reveal the advantages of the auxetic area for PEH. Although it lacks an auxetic zone, it utilizes a simple bulk substrate with the exact outward dimensions as AS-I and AS-II. The epoxy coating covers the entire area underneath the PZT element, and a plain bonded them to the substrate beam.

Additionally, the influence of geometry parameters on the harvested power is investigated, and the dimensions are selected to generate maximum output power based on the findings. Also, the effect of different factors like electrical resistance, load magnitude, frequency, and bonding strength on the PEH performance of the systems are analyzed. Therefore, under a comprehensive parametric analysis, the optimum dimensions and factor values for the proposed auxetic model are reported resulting in maximum extracted power while preserving peak stress within the material strength limitation, with a 1.1 safety factor. The parameters examined comprise: fillet radius, side angle, ligament width, the width of the rectangular hole, side length cell angle, length of the rectangular hole, and substrate thickness all exhibited in Figure 2. Table 1 provides a list of the studied ranges and the optimized values for these parameters. Besides, the impact of using different PZT materials on the peak stress and output power in the desired frequency range of ($1-20\mathrm{Hz}$) has been studied. Accordingly, the proposed model has been optimized by selecting the best option. Regarding the FEM discretization models, the tetrahedral-triangular mesh element type is employed, and the mesh quality is determined for each model through the mesh convergence study. The elements type is tetrahedral on the beam and substrate, while PZT and epoxy faces include triangular elements that are swept across their domains. Table 4 presents the mesh properties selected for the models used in the PEH study.

On top of that, FE modeling with COMSOL Multiphysics® 6.0 is utilized for calculating the PR and examining the auxetic behavior and stress distribution of different models. Figure 1 depicts the FE models used for the PR analysis. The PR values are calculated under the solid mechanic domain with stationary study facing an axial excitation force of $2.5e^5\mathrm{N}/\mathrm{m}^3$ while the axial bottom surface is fixed. Free boundary conditions are applied to the two lateral sides. The selected mesh is a tetrahedral mesh type for the FEM models in the PR simulations. Table 6 details the mesh properties determined for the models used in the PR study. Finally, COMSOL Multiphysics computes the PR using Eq. (9). Furthermore, the effect of structural parameters on PR value has been studied. In this regard, we can compare the trend of changing harvested power rate with the PR rate as a function of structural

parameters. In addition, this work aligns with the current promising trend in various industries of utilizing lightweight structures. Consequently, the models are evaluated and compared based on their lightness.

6. Results and discussion

The AS-II booster with optimized structural parameters is capable of producing $5.43\ \mu\mathrm{W}$ electric power at $10\ \mathrm{Hz}$ with a combination of $R = 378\ \mathrm{K\Omega}$, $k_a = 220\ \mathrm{GN/m^3}$ and $f_s = 0.9e^6\mathrm{N/m^3}$, while the AS-I booster and the plain harvester generate $2.37\ \mu\mathrm{W}$ and $0.35\ \mu\mathrm{W}$ power at $10\ \mathrm{Hz}$ under the same combination. Under the optimum pair of $R = 250\ \mathrm{K\Omega}$, $k_a = 200\ \mathrm{GN/m^3}$, the AS-II booster can produce $6.71\ \mu\mathrm{W}$ electric power $10\ \mathrm{Hz}$, while the AS-I booster and the plain harvester generate $2.98\ \mu\mathrm{W}$ and $0.46\ \mu\mathrm{W}$ power at $10\ \mathrm{Hz}$ for the low incident vibration level of $0.9e^6\mathrm{N/m^3}$. As a result, the AS-II booster exhibits a magnification factor of 14.61 and 2.25 times power gain with respect to the AS-I and plain substrate harvesters, respectively. Considering high incident vibration levels ($f_s = 2.3e^6\mathrm{N/m^3}$), the AS-II booster with optimized structural parameters is capable of producing $43.84\ \mu\mathrm{W}$ electric power at $10\ \mathrm{Hz}$ with an optimum pair of $R = 250\ \mathrm{K\Omega}$, $k_a = 250\ \mathrm{GN/m^3}$, while the AS-I booster and the plain harvester generate $19.48\ \mu\mathrm{W}$ and $3\ \mu\mathrm{W}$ power at $10Hz$ under the same combination. This will give a magnification factor of 14.61 and 2.25 times power gain, concerning the AS-I and plain substrate harvesters, respectively. It can be concluded that under different incident vibration levels, the power gain factor will approximately stay constant [49].

A comparison of our proposed model with the available ones is provided in Table 3 in terms of mechanism approaches and PEH performance. Including studies conducted by Askari et al. [30], Moayedizadeh [38], Eghbali et al. [45, 63], where they employed a designed booster to improve the PZT performance in a cantilever beam-type energy harvester. It can be observed that our presented booster can effectively improve the PEH system's performance with a significant power gain factor at a low target frequency while the structure size is relatively small. The reason for such outstanding performance can be explained by the geometry properties where the proposed auxetic region can concentrate most portion of the mechanical energy and stress under the PZT element, compared to other available models.

Table 3. Assessment of the PEH system's performance of our proposed study with other available booster structures.

Display Table

It is vital to validate the FE model using the mesh convergence technique (MCT) to achieve optimal mesh quality. MCT ensures that after the optimal mesh grades, there is no significant change in the simulation results by increasing mesh quality. Figure 4(a) displays the mesh convergence graphs. It can be observed that while adding more elements, the calculated powers monotonically approach final values of $43.84\ \mu\mathrm{W}$, $19.48\ \mu\mathrm{W}$, and $3\ \mu\mathrm{W}$ for AS-II, AS-I, and the plain substrate, respectively. The number of degrees of freedom (DoF) and the percentage error for each case are reported in Table 4. In addition to checking the numerical convergence, the FEM outcomes

experimental data of AS-I under tension with a harmonic strain of $250\ \mu\varepsilon$. Table 5 demonstrates that our calculated FEM results agreed well with the measured experimental data possessing an error rate below 2%.

Figure 4. Mesh convergence plots, concerning the included number of degrees of freedom: (a) corresponding to the power calculation and (b) corresponding to PR calculation.

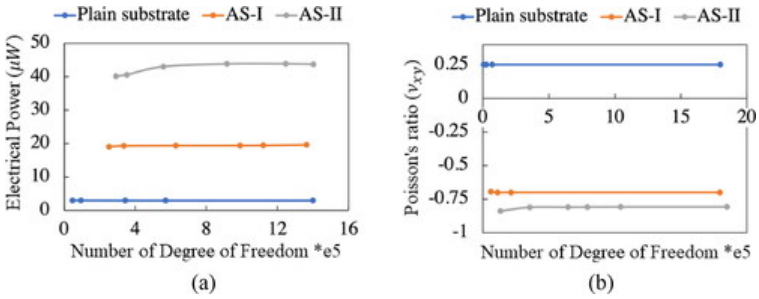

Display full size

Table 4. Mesh properties for PEH study.

Download CSV Display Table

Table 5. Validation of the numerical simulation.

Display Table

Furthermore, Figure 5 illustrates the auxetic behavior of AS-I and AS-II. One can notice that the structures expand when subjected to a tensile force in the axial direction. The PR results show that the AS-II with optimized structural parameters based on the PEH study exhibits an NPR of -0.8, while its value could vary from -2 to 0. The AS-I and steel plain show a PR rate of -0.7 and 0.25, respectively. Table 6 lists the appropriate number of DoF for each case where MCT is applied to the FEM models for PR analysis. Based on the MCT analysis, the PR simulation outcomes are independent of mesh quality. The mesh convergence plots are displayed in Figure 4(b).

Figure 5. Illustration of auxetic behavior. (I) Corresponding to the as-I booster and (II) corresponding to one single unit cell of the as-II booster.

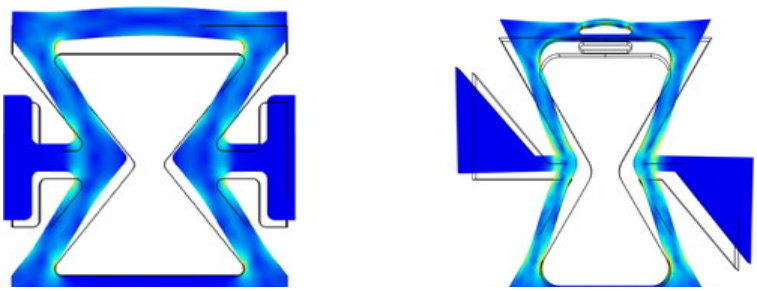

Display full size

Table 6. Mesh properties for PR study.

Download CSV Display Table

According to the simulation process, the FEM provided precise results that were validated using available experimental data. However, the computational time and complexity become a concern when the mesh quality consists of high DoF, particularly in the coupling domain between solid mechanics and piezoelectric circuits, where the power generated needs to be calculated. To address this challenge, the CUF can be an efficient solution to deal with computational costs in the simulation. By extending the unknown variables over the beam cross section, mathematical models can be created. The displacement field in the CUF can be uniformly estimated using a series of expansion or interpolation polynomials, in which both Taylor-like and Lagrange polynomials can be employed to develop mathematical models. For example, Wu et al. [65] analytically calculated frequency response for the Rayleigh wave propagation across a periodic elastic substrate coated with a T-plate utilizing CUF. The study compared the CUF results to those obtained by COMSOL software, indicating the reliability and accuracy of CUF as a computationally simpler and less complex alternative. However, it is a challenge to use CUF for a 3D multi-body PEH structure to calculate power harvested and mechanical properties under coupled mechanics and piezo-electrical circuits resulting from incident waves or impact loads. Researchers should consider the benefit of CUF-based techniques for their future work so that CUF can facilitate them to study the problem under a wider frequency range while giving efficient and accurate results with less computational time and making future studies more realistic.

A parametric study has been conducted on the AS-II to evaluate the influence of different geometry parameters on extracted power under a body load of $0.9e^6\mathrm{N}\ /\ \mathrm{m}^3$, and the system's auxetic behavior. Figure 6(I) presents the variation of harvested electrical power and NPR as a function of α. Increasing α would shift NPR to more negative values, but decrease harvested electrical power. On the other hand, Figure 6(II) illustrates that increasing d would enhance the harvested power until it reaches its maximum value at $d = 0.3\mathrm{mm}$. However, it shifts NPR to more negative values until it hits the minimum value at $d = 0.3\mathrm{mm}$. In Figure 6(III), growing r has boosted extracted power and the NPR values. This investigation demonstrates that variations in geometry parameters affect both the harvested electrical power and auxetic behavior. Additionally, there is no comprehensive relationship between the trend of changing harvested power and NPR rates that can be applied to all geometrical modifications. As a result, the optimization of geometry parameters plays a crucial role in improving the mechanical and electrical performances of the system to select the best matching scheme of the NPR and harvested power values.

Figure 6. Influence of geometrical parameters: (I) α (II) d and (III) r on the extracted electrical power and the PR.

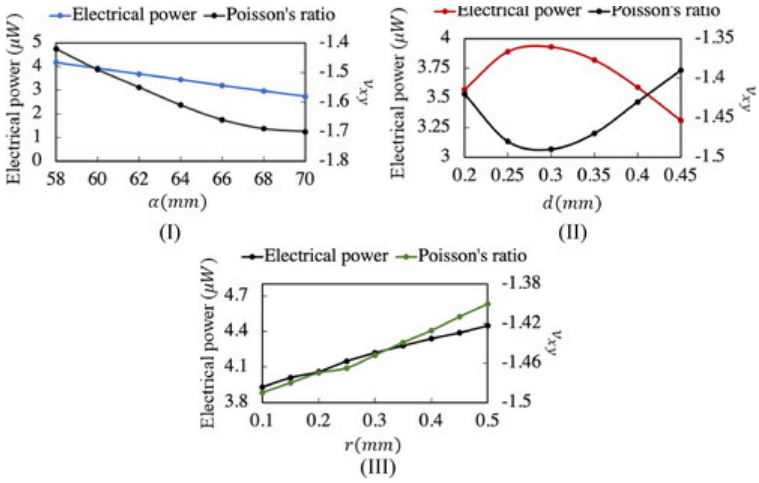

Display full size

In addition, the evolution of harvested power and NPR as a function of a and b are provided in Figure 7. It is evident from Figure 7(I) that harvesting electrical power has been increasing by decreasing a and b. The same trend can be seen in Figure 7(II), where lowering a and b increases the system's capacity for auxetic deformation. Besides, power and NPR are located at $a = 0.15\,\mathrm{mm}$ and $b = 1\,\mathrm{mm}$. Figure 8 displays the evolution of harvested electrical power and NPR for varying L and θ. It is observed that power production grows by increasing L and θ. Nevertheless, lowering L and θ strengthens the auxetic capacity of the system. $\theta = 40^{\circ}$ and $L = 2\,\mathrm{mm}$ are the positions of the peak power.

Figure 7. Influence of geometrical parameters a and b : (I) on the extracted electrical power and (II) on the PR.

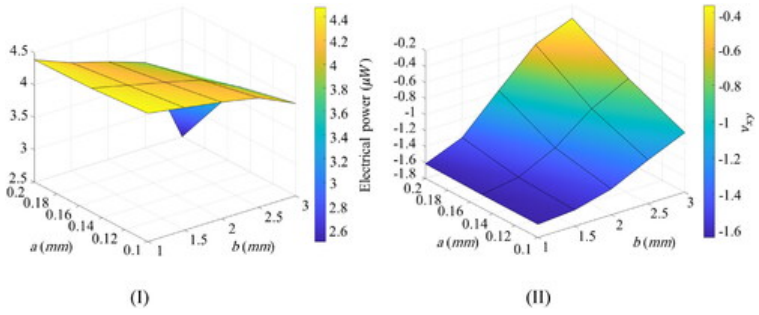

Display full size

Figure 8. Influence of geometrical parameters L and θ: (I) on the extracted electrical power and (II) on the PR.

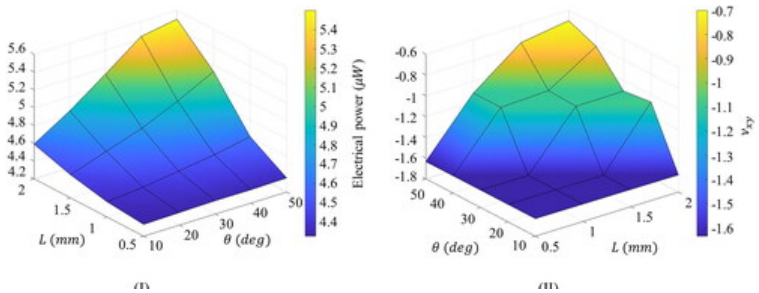

Display full size

Furthermore, Figure 9 depicts the electrical power map based on varying substrate thickness under different R. Results indicate that the optimum pair of $R = 250\mathrm{K}\Omega$ and t_s between $(1.5 - 1.8\mathrm{mm})$ generates electrical power up to $6.1\ \mu\mathrm{W}$. Moreover, the influence of increasing t_s on the system's auxetic deformation is investigated. Figure 10 indicates that by increasing t_s, there has been a slight increase in the PR. It can be mainly attributed to the increasing structure stiffness. The ability of the structure to deform would fall due to increasing thickness, which would enrich structure stiffness. As a result, the auxetic behavior would be lessened. The impact of several elements, such as electrical resistance, load magnitude, frequency, and bonding strength, on the PEH performance of the systems is examined in the following section. Figure 11 illustrates the impact of the frequency and magnitude of the load on the power output. It can deduce that increasing the magnitude of the applied load and frequency can dramatically lead to expanded power output.

Figure 9. Power map based on different values of thickness t_s and electrical resistance R.

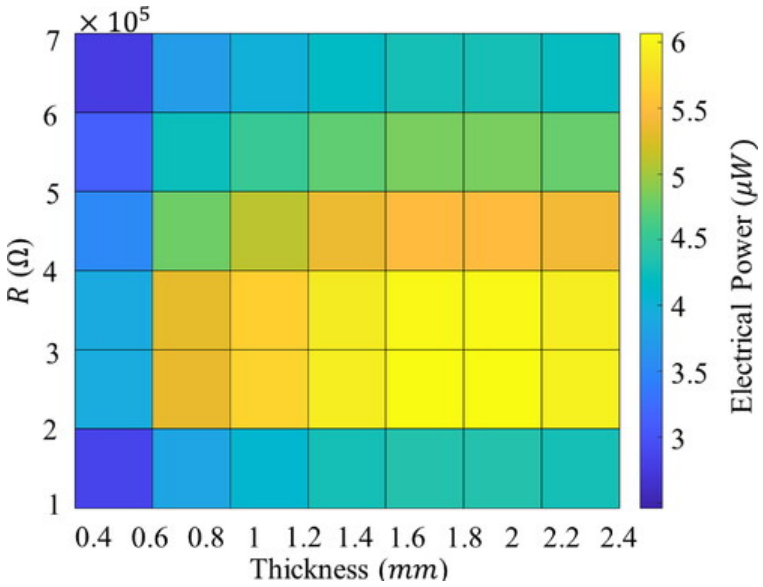

Display full size

Figure 10. Influence of thickness t_{as} and t_s on the PR.

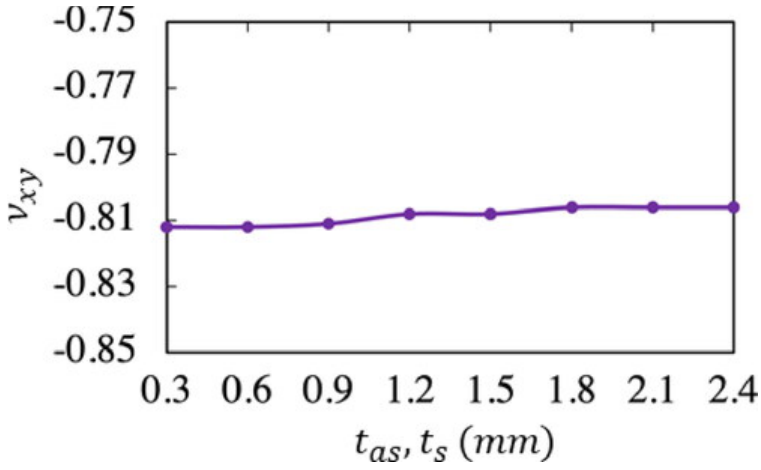

Display full size

Figure 11. Power map based on different magnitudes of the applied force and the values of frequency.

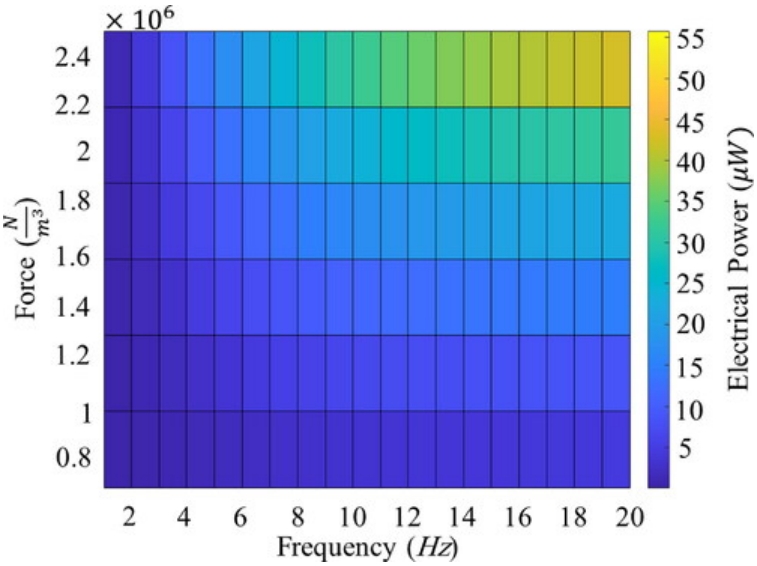

Display full size

Figure 12 presents the harvested electrical power variation with respect to increasing load resistance for three case studies. In all examples, the highest power output is observed at $R = 250K\Omega$, after which there is a significant decrease in value. Figure 13 illustrates the harvested power variation as a function of bonding stiffness k_a. It has been shown that raising k_a would result in a considerable increase in power production. According to numerical results, the PEH performance of the system is significantly influenced by the adhesive bonding strength. The diagram related to AS-II increases the power output with a sharper slope than AS-I and plain substrate. The strain from the substrate is transferred to the PZT component through the epoxy layer with greater effectiveness when higher values of k are implemented. For example, in the case of $k_a = 500\ \mathrm{GN/m^3}$, the harvested power is 73 $\mu\mathrm{W}$ in AS-II, 37.5$\mu\mathrm{W}$ in AS-I, and 7.5$\mu\mathrm{W}$ in the plain substrate. Additionally, it can be observed that the AS-II design performs better across the board for all bonding strength levels. Later on, we will discuss in detail the modified stress distribution responsible for this improvement in efficiency.

Figure 12. Extracted electrical power as a function of load resistance R, for the case of plain substrate, as-I, and as-II harvester models. All points use the same excitation of $2.3e^6\mathrm{N/m^3}$ at $10\ \mathrm{Hz}$.

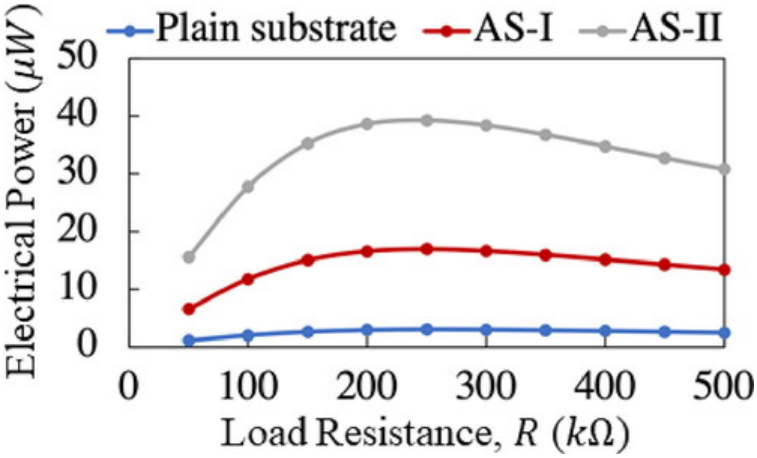

Display full size

Figure 13. Extracted electrical power as a function of spring constant per unit area k_a, in the TEL of the plain substrate, AS-I, and AS-II harvester models. All points use the same excitation of $2.3e^6\mathrm{N}\ /\ \mathrm{m^3}$ at $10\ \mathrm{Hz}$.

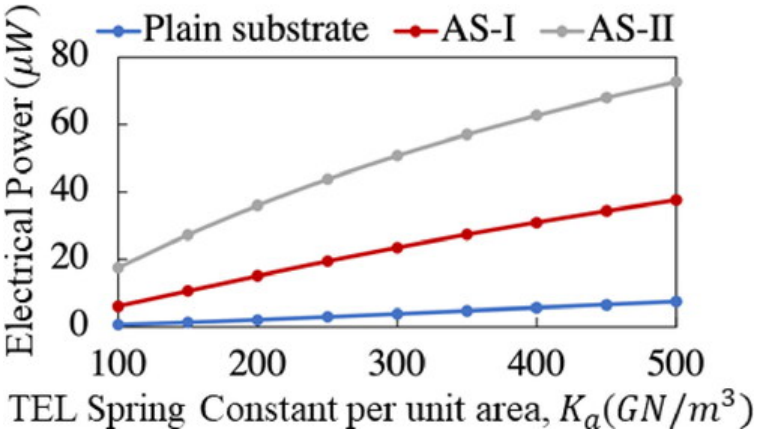

Display full size

The stress distribution over the PZT layer has been measured and compared in order to investigate the origins of such disparate responses to the same load input. The harvested power is proportional to longitudinal and perpendicular stress in the PZT layer as shown in Eq. (5):

According to this equation, the amount of harvested power is determined based on the average stress in both longitudinal and lateral tendencies. Conventional plain harvesters with positive PR possess axial and later stress with the opposite sign due to the axial tension causing compression in the lateral direction. Conversely, when a PZT patch is bonded to an auxetic structure, the axial and lateral stress will have the same sign as the axial tension, resulting in an expansion in the lateral direction. Consequently, they can be either negative or positive, simultaneously, which can generate higher electrical power. Figure 14 depicts the stress distribution over the PZT layer in different boosters. It is observed that the PZT layer in the plain harvester has lower peak and average stresses than the other two auxetic boosters, which limits the rate of harvested electric power. The traditional plain

On the other hand, the AS-I booster focuses stress and strain on the more flexible auxetic part, particularly on the corners that bend outward. However, most regions remain at low-stress levels. Moreover, the AS-II booster distributes stress more over the connections and perforation parts made by the auxetic area, and unlike AS-I, most regions remain under relatively high-stress levels. The peak stress of $262\mathrm{MPa}$ in the AS-II substrate was, therefore, discovered at the center of the auxetic area. This stress is sufficiently below the yield strength of $286\mathrm{MPa}$ of the substrate with a safety factor of 1.1. Additionally, for AS-I and bulk plain, the substrate's peak stress is $108\mathrm{MPa}$ and $14\mathrm{MPa}$, respectively. Likewise, the maximum stress experienced by the PZT component in AS-II was approximately $16.72\mathrm{MPa}$, which is sufficiently below its tensile strength of $115\mathrm{MPa}$. This value is $12\mathrm{MPa}$ and $1.6\mathrm{MPa}$ in AS-I and the plain substrate, respectively. In addition, the average stress around the PZT layer in the AS-II harvester is $5.04\mathrm{MPa}$, while in AS-I and the conventional plain substrate are $2.28\mathrm{MPa}$ and $0.77\mathrm{MPa}$, respectively. Comparing the results shows that AS-II can highly concentrate stress and isolate the majority of incident vibrations into its auxetic region and subsequently transfer it to the PZT patch through the epoxy layer. This phenomenon will increase the power output according to Eq. (5). Figure 15 illustrates the level of maximum distributed stress in the PZT element as a function of k_a. It can be seen that the maximum PZT stress gradually increases with growing k_a. However, the maximum stress in substrates would remain approximately constant beyond $k_a = 200\ \mathrm{GN/m^3}$. The reason behind such improvement is that while the bonding strength increases, the epoxy layer effectively transfers strain and distributed stress from the substrate to the PZT element. As a result, the maximum stress in the PZT layer and, therefore, the power output (based on Eq. (5)) will be improved. It can be found that the auxetic pattern boosts the maximum stress and mean stress over the PZT component, and the AS-II booster has the highest values of both when compared to other models. In fact, improving bonding strength and principal stress in the PZT layer are two parallel promoters for harvested power enhancement.

Figure 14. Stress distribution over the PZT layer. (a) corresponding to the plain substrate, (b) corresponding to the as-I booster, and (c) corresponding to the as-II booster.

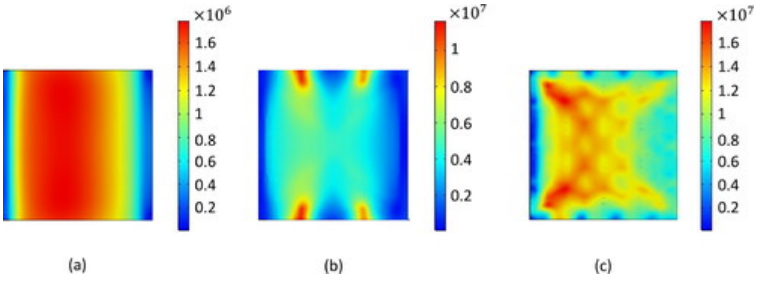

Display full size

Figure 15. Peak stress as a function of spring constant per unit area k_a, in the piezo layer, and substrate of the plain structure, AS-I, and AS-II harvester models. All points use the same excitation of $2.3e^6\mathrm{N/m^3}$ at $10\ \mathrm{Hz}$.

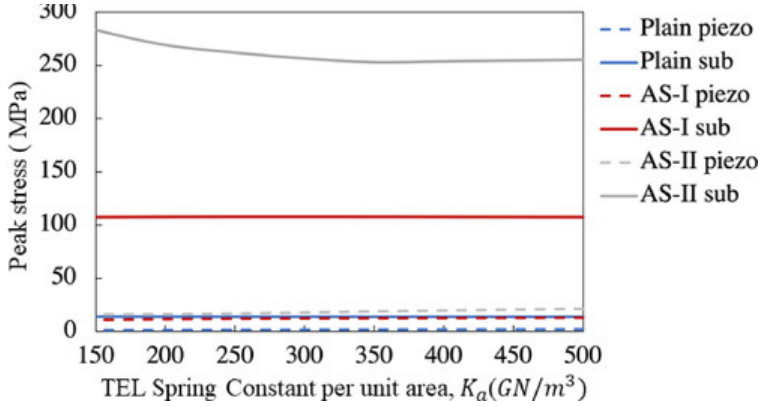

Display full size

Furthermore, the stress distribution obtained by PR analysis under a body load of $2.5e^5 N / m^3$ is studied on different substrates. Figure 16 depicts the stress distribution of steel plate, AS-I booster, and AS-II booster. It has been shown that AS-I and AS-II boosters exhibited auxetic behavior as they expanded laterally under axial tensile force. Conversely, the plate exhibits conventional positive PR behavior as it is shrunk laterally under axial tensile load. The reports determined that the AS-II booster has a maximum stress of 33MPa with an NPR of -0.80. Also, the peak stress and PR in the AS-I booster are 14.75MPa and -0.70, while in the plain substrate are 0.39 MPa and 0.253. The PR and FEM results reveal that the AS-II booster can significantly absorb and concentrate incident excitations based on its auxetic behavior and transfer them into the PZT layer more efficiently. This phenomenon will own a positive effect on the harvested power based on Eq. (5).

Figure 16. Stress distribution of different substrate boosters. (a) Corresponding to the plain substrate, (b) corresponding to the as-I booster, and (c) corresponding to the as-II booster.

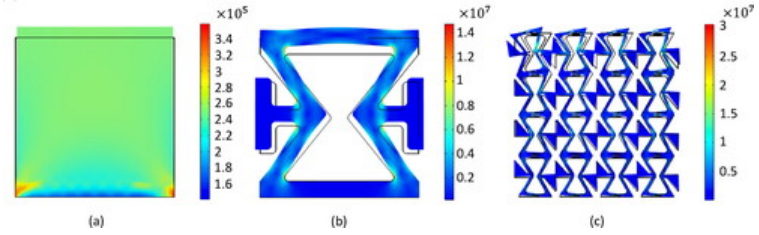

Display full size

The type of PZT material is another promising parameter that needs to be assessed when conducting the parametric analysis. Figure 17 displays the frequency-dependent impact of using different PZT types. From the graph, we can see that the PZT-5H has the best performance among the investigated materials. Also, the harvested power as a function of frequency for the incident low and high vibrations is provided in Figure 18. It is obvious that the AS-II harvester outperforms the other traditional harvesters in both low- and high-vibration attenuations. We could gain a magnification factor of 14.61 and 2.25 for AS-II compared to harvested power by the plain substrate and AS-I, respectively. It can also be noticed that the magnification factor is constant under different input vibration levels. This observation demonstrates that the magnification factor is a product of the substrate geometry rather than the excitement. According to the current policy followed by industrial sectors, the provided models (shown in Figure 1) are studied based on their structure's weight. Results indicate that the AS-II booster is sufficiently

other words, the AS-II booster exhibits a lightness position of 5.83 times (or 82.87%) lighter than the conventional plain one, and 3.16 times (or 68.36%) than the AS-I booster. To wrap up the letter, an overview of different systems' performance is provided in Table 7. It can result that the AS-II booster has the most effective performance in terms of various factors, including power output, stress distribution, lightweight, and auxetic behavior.

Figure 17. Influence of the PZT type on the output electrical power concerning the frequency.

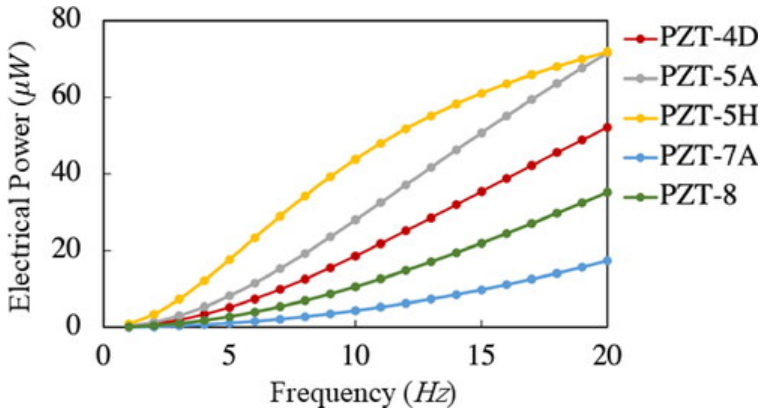

Display full size

Figure 18. Harvested power as a function of frequency for the plain substrate, as-I, and as-II harvesters: (a) corresponding to the case with an excitation $0.9e^6\mathrm{N}/\mathrm{m}^3$ at $10\ \mathrm{Hz}$. (b) Corresponding to the case with an excitation of $2.3e^6\ \mathrm{N}/\mathrm{m}^3$ at $10\ \mathrm{Hz}$.

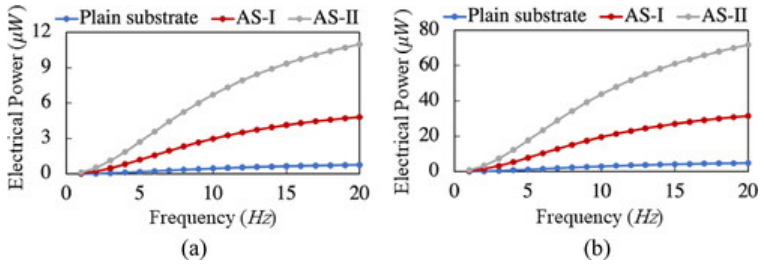

Display full size

Table 7. Comparison of different systems' performance under the excitation of $2.3e^6\mathrm{N}/\mathrm{m}^3$ at $10\mathrm{Hz}$ with $R = 378\ \mathrm{K\Omega},\ k_a = 220\ \mathrm{GN}/\ .\ \mathrm{m}^3$

Display Table

7. Conclusion

According to the literature, PZT patches own a low-efficiency rate when extracting incident vibrations at low frequencies, leading to a significant obstacle in their practical usage. As a consequence, the use of such PZT

energy in practice unless the input vibration level is sufficiently high. Another essential concern is ensuring that the system performs efficiently near the resonance frequency range of the acoustic/elastic metamaterial booster, beyond which the system's performance will considerably diminish, resulting in the disappearance of most incident energy waves. In an effort to address the mentioned difficulties, the current study proposed a novel auxetic metamaterial booster for VEH with PZT point defects, which has employed various mechanisms, including re-entrant, chiral, honeycomb supercell, and perforations.

The FE method was utilized to perform modeling and simulations in this work, and numerical results are validated by MRT and available experimental data. Based on stress distribution and auxetic mechanism, the present auxetic booster can sufficiently improve PEH regardless of BGs and resonance frequency. A comprehensive parametric study has been conducted on the proposed model to investigate the effect of geometry and type of PZT material on PEH performance. We further examined the impact of various factors, such as load resistance, frequency, amplitude of excitation, and bonding strength, on the harvested power. In such a manner, The AS-II was optimized using the parametric results and analyzed for its PEH performance compared with two conventional vibration energy harvesters, namely plain substrate and auxetic booster AS-I. Calculations were conducted under low and high incident vibrations within the desired extremely low-frequency range of $1-20\ \mathrm{Hz}$. Results demonstrate a magnification factor of 14.61 and 2.25 for AS-II compared to harvested power by the plain substrate and AS-I, respectively. The logic behind the outstanding performance of the auxetic mechanism is explained by investigating stress distribution and bonding stiffness. Results show that AS-II can trap most portion of the incoming vibrations by its unique geometry and focus the stress inside its auxetic region. Substantially, it can profoundly maximize stress and strain distributions effectively more into the PZT layer. This phenomenon opens up the possibility of generating electrical power from smaller amplitude vibrations, drawing these configurations suited to structural health monitoring.

In addition, the effect of geometry parameters on the PR is analyzed in AS-II, and the auxetic behavior of presented boosters is studied using PR analysis. Displacement vector fields indicate the model's response under tensile load where AS-I and AS-II exhibit typical auxetic behavior with NPR property. The present harvester is strain controllable, where it can set PR between -2 to 0, resulting in robust PEH even if switching input vibration from high to low levels. This novel idea allows us to serve cantilever-type resonators at frequencies far lower than their resonant frequencies.

Concerning the current policy of utilizing lightweight structures, the presented boosters are compared based on contained weight. The AS-II booster shows a lightness position of 5.83 times (or 82.87%) lighter than the conventional plate and 3.16 times (or 68.36%) than the AS-I booster. This study shows that AS-II is superior among available harvesters in terms of PEH and lightness. The proposed concept is reliable and applicable for self-power and wireless sensors in industry and IOT network environments.

8. Future perspectives

As part of our future work, we aim to create an auxetic piezo-metamaterial harvester device based on the proposed model in this study. The device will be practically evaluated using experimental testing and has great potential for use in VEH applications within the railway system. To achieve this, we plan to extend the CUF to cover

harvested and mechanical features of the device while reducing computational costs. Additionally, we will validate the analytical results with an experimental test.

Ethics statement

The content presented here is the result of the author's original work, which has not been published elsewhere before and is not currently being considered for publication elsewhere. The paper reflects the author's own research and analysis in a truthful and complete manner, and the paper properly credits the meaningful contributions of coauthors and coresearchers.

Disclosure statement

No potential conflict of interest was reported by the author(s).

Data availability statement

All data included in this manuscript are available upon a reasonable request by contacting the corresponding author.

Additional information

Funding

This research received financial support from the Research Office of Iran University of Science and Technology (Grant number 160-19711) for the research and authorship of this article.

References

1. H. Askari, E. Asadi, Z. Saadatnia, A. Khajepour, M. B. Khamesee, and J. Zu, A hybridized electromagnetic-triboelectric self-powered sensor for traffic monitoring: concept, modelling, and optimization, Nano Energy, vol. 32, pp. 105–116, 2017. DOI: 10.1016/j.nanoen.2016.12.024.

Web of Science ® | Google Scholar

2. Q. Duan, W. Peng, J. He, Z. Zhang, Z. Wu, Y. Zhang, S. Wang, and S. Nie, Rational design of advanced triboelectric materials for energy harvesting and emerging applications, Small Methods, vol. 7, no. 2, pp. e2201251, 2023. DOI: 10.1002/smtd.202201251.

PubMed | Web of Science ® | Google Scholar

3. H. Wang, C. He, S. Lv, and H. Sun, A new electromagnetic vibrational energy harvesting device for swaying cables, Appl. Energy, vol. 228, pp. 2448–2461, 2018. DOI: 10.1016/j.apenergy.2018.07.059.

Web of Science ® | Google Scholar

4. P. Kakou and O. Barry, Simultaneous vibration reduction and energy harvesting of a nonlinear oscillator using a nonlinear electromagnetic vibration absorber-inerter, Mech. Syst. Sig. Process., vol. 156, pp. 107607, 2021. DOI: 10.1016/j.ymssp.2021.107607.

Web of Science ® | Google Scholar

5. P. Firoozy and S. Ebrahimi-Nejad, Broadband energy harvesting from time-delayed nonlinear oscillations of magnetic levitation, J. Intell. Mater. Syst. Struct., vol. 31, no. 5, pp. 737–755, 2020. DOI: 10.1177/1045389X19898751.

Web of Science ® | Google Scholar

6. S. Ebrahimi-Nejad and M. Boreiry, Comprehensive nonlocal analysis of piezoelectric nanobeams with surface effects in bending, buckling and vibrations under magneto-electro-thermo-mechanical loading, Mater. Res. Exp., vol. 5, no. 3, pp. 035028, 2018. DOI: 10.1088/2053-1591/aab46d.

Web of Science ® | Google Scholar

7. J. Marzbanrad, S. Ebrahimi-Nejad, G. Shaghaghi, and M. Boreiry, Nonlinear vibration analysis of piezoelectric functionally graded nanobeam exposed to combined hygro-magneto-electro-thermo-mechanical loading, Mater. Res. Exp., vol. 5, no. 7, pp. 075022, 2018. DOI: 10.1088/2053-1591/aad0ce.

Web of Science ® | Google Scholar

8. A. Shokuhfar, P. Heydari, M.R. Aliahmadi, M. Mohtashamifar, S. Ebrahimi-Nejad, and M. Zahedinejad, Low-cost polymeric microcantilever sensor with titanium as piezoresistive material, Microelectron. Eng., vol. 98, pp. 338–342, 2012. DOI: 10.1016/j.mee.2012.07.067.

Web of Science ® | Google Scholar

9. M. Safaei, H.A. Sodano, and S.R. Anton, A review of energy harvesting using piezoelectric materials: state-of-the-art a decade later (2008–2018), Smart Mater. Struct., vol. 28, no. 11, pp. 113001, 2019. DOI: 10.1088/1361-665X/ab36e4.

Web of Science ® | Google Scholar

10. S. Ebrahimi-Nejad and M. Kheybari, Composite locally resonating stop band acoustic metamaterials, Acta Acust. United Acust., vol. 105, no. 2, pp. 313–325, 2019. DOI: 10.3813/AAA.919314.

Web of Science ® | Google Scholar

11. S. Ebrahimi-Nejad and M. Kheybari, Honeycomb locally resonant absorbing acoustic metamaterials with stop

Web of Science ® | Google Scholar

12. Y. Chen, X. Fang, J. Wang, M. Filippi, and E. Carrera, An analysis of band gap characteristics of metamaterial plates with dual helix cells, Mech. Adv. Mater. Struct., pp. 1–11, 2023. DOI: 10.1080/15376494.2023.2218361.

Google Scholar

13. M. Kheybari and S. Ebrahimi-Nejad, Locally resonant stop band acoustic metamaterial muffler with tuned resonance frequency range, Mater. Res. Exp., vol. 6, no. 2, pp. 025802, 2018. DOI: 10.1088/2053-1591/aaed4b.

Web of Science ® | Google Scholar

14. M. Kheybari and S. Ebrahimi-Nejad, Dual-target-frequency-range stop-band acoustic metamaterial muffler: acoustic and CFD approach, Eng. Res. Exp., vol. 3, no. 3, pp. 035027, 2021. DOI: 10.1088/2631-8695/ac1989.

Google Scholar

15. Z.-Q. Lu, L. Zhao, H. Ding, and L.-Q. Chen, A dual-functional metamaterial for integrated vibration isolation and energy harvesting, J. Sound Vib., vol. 509, pp. 116251, 2021. DOI: 10.1016/j.jsv.2021.116251.

Web of Science ® | Google Scholar

16. F. Hou, S. Xiao, and H. Wang, Mechanical properties characterization and zero Poisson's ratio design for perforated auxetic metamaterial by computational homogenized method, Mech. Adv. Mater. Struct., vol. 29, no. 28, pp. 7640–7651, 2022. DOI: 10.1080/15376494.2021.2004268.

Web of Science ® | Google Scholar

17. F. Jiang, S. Yang, C. Qi, and C. Ding, Quasi-static crushing response of additive manufactured 3d reentrant circular auxetics with different polymer matrices, Mech. Adv. Mater. Struct., vol. 30, no. 18, pp. 3826–3846, 2023. DOI: 10.1080/15376494.2022.2084193.

Web of Science ® | Google Scholar

18. J. Jin, S. Jiang, and H. Hu, Multiple wide band gaps in a convex-like holey phononic crystal strip, Rev. Adv. Mater. Sci., vol. 61, no. 1, pp. 68–78, 2022. DOI: 10.1515/rams-2022-0010.

Web of Science ® | Google Scholar

19. K. H. Sun, J. E. Kim, J. Kim, and K. Song, Sound energy harvesting using a doubly coiled-up acoustic metamaterial cavity, Smart Mater. Struct., vol. 26, no. 7, pp. 075011, 2017. DOI: 10.1088/1361-665X/aa724e.

Web of Science ® | Google Scholar

20. K.-J. Liu, H.-T. Liu, J. Li, and F.-G. Ren, Tunable thermal expansion and bandgap properties of the bi-material-directional honeycomb metamaterial, Mech. Adv. Mater. Struct., pp. 1–15, 2022. DOI: 10.1080/15376494.2022.2154875.

21. M. Yari and E. Ghavanloo, In-plane elastic properties of meta-chiral star-shaped lattice structure, Mech. Adv. Mater. Struct., pp. 1–8, 2023. DOI: 10.1080/15376494.2023.2206820.

View | Web of Science ® | Google Scholar

22. S. Farhangdoust, G. Georgeson, J.-B. Ihn, and F.-K. Chang, Kirigami auxetic structure for high efficiency power harvesting in self-powered and wireless structural health monitoring systems, Smart Mater. Struct., vol. 30, no. 1, pp. 015037, 2021. DOI: 10.1088/1361-665X/abcaaf.

View | Web of Science ® | Google Scholar

23. K. Yi, Z. Liu, and R. Zhu, Multi-resonant metamaterials based on self-sensing piezoelectric patches and digital circuits for broadband isolation of elastic wave transmission, Smart Mater. Struct., vol. 31, no. 1, pp. 015042, 2022. DOI: 10.1088/1361-665X/ac3b1f.

View | Web of Science ® | Google Scholar

24. K. Ma, T. Tan, Z. Yan, F. Liu, W.-H. Liao, and W. Zhang, Metamaterial and Helmholtz coupled resonator for high-density acoustic energy harvesting, Nano Energy, vol. 82, pp. 105693, 2021. DOI: 10.1016/j.nanoen.2020.105693.

View | Web of Science ® | Google Scholar

25. C. Wang, L. Cai, M. Gao, L. Jin, L. Sun, X. Tang, G. Shi, X. Zheng, and C. Guo, Manufacturing of membrane acoustical metamaterials for low frequency noise reduction and control: a review, Mech. Adv. Mater. Struct., pp. 1–16, 2023. DOI: 10.1080/15376494.2023.2242363.

View | Web of Science ® | Google Scholar

26. A. Kitagawa and J. Sakai, Bloch theorem in cylindrical coordinates and its application to a Bragg fiber, Phys. Rev. A., vol. 80, no. 3, Article no. 033802, 2009. DOI: 10.1103/PhysRevA.80.033802.

View | PubMed | Web of Science ® | Google Scholar

27. M. Ravanbod and S. Ebrahimi-Nejad, Innovative lightweight re-entrant cross-like beam phononic crystal with perforated host for broadband vibration attenuation, Appl. Phys. A., vol. 129, no. 2, Article no. 102, 2023. DOI: 10.1007/s00339-022-06339-6.

View | Web of Science ® | Google Scholar

28. T.-X. Ma, Q.-S. Fan, Z.-Y. Li, C. Zhang, and Y.-S. Wang, Flexural wave energy harvesting by multi-mode elastic metamaterial cavities, Extreme Mech. Lett., vol. 41, pp. 101073, 2020. DOI: 10.1016/j.eml.2020.101073.

View | Web of Science ® | Google Scholar

29. W. Sun, K. Zhong, Y. Liu, H. Xiao, D. Zhao, Z. Yan, and T. Tan, Enhanced metamaterial vibration for high-performance acoustic piezoelectric energy harvesting, Compos. Commun., vol. 35, pp. 101342, 2022. DOI: 10.1016/j.coco.2022.101342.

30. M. Askari, E. Brusa, and C. Delprete, Design and modeling of a novel multi-beam piezoelectric smart structure for vibration energy harvesting, Mech. Adv. Mater. Struct., vol. 29, no. 28, pp. 7519–7541, 2022. DOI: 10.1080/15376494.2021.2001122.

View | Web of Science ® | Google Scholar

31. B. Zhao, H.R. Thomsen, J.M. De Ponti, E. Riva, B.V. Damme, A. Bergamini, E. Chatzi, and A. Colombi, A graded metamaterial for broadband and high-capability piezoelectric energy harvesting, Energy Convers. Manag., vol. 269, pp. 116056, 2022. DOI: 10.1016/j.enconman.2022.116056.

View | Web of Science ® | Google Scholar

32. X. Wu, Y. Jin, A. Khelif, X. Zhuang, T. Rabczuk, and B. Djafari-Rouhani, Topological surface wave metamaterials for robust vibration attenuation and energy harvesting, Mech. Adv. Mater. Struct., vol. 29, no. 26, pp. 4759–4767, 2022. DOI: 10.1080/15376494.2021.1937758.

View | Web of Science ® | Google Scholar

33. S. Raghavan, A. Sharma, and R. Gupta, Resonant frequency tuning of a novel piezoelectric vibration energy harvester (PVEH), Mech. Adv. Mater. Struct., pp. 1–16, 2023. DOI: 10.1080/15376494.2023.2209078.

View | Web of Science ® | Google Scholar

34. M. Rezaei, R. Talebitooti, and M.I. Friswell, Efficient acoustic energy harvesting by deploying magnetic restoring force, Smart Mater. Struct., vol. 28, no. 10, pp. 105037, 2019. DOI: 10.1088/1361-665X/ab3a6a.

View | Web of Science ® | Google Scholar

35. W. Jiang, Y. Ao, J. Liu, J. Liu, and W. Huang, Dynamic responses and failure mechanism of composite double-arrow auxetic structure under impact loading, Mech. Adv. Mater. Struct., vol. 30, no. 13, pp. 2593–2609, 2023. DOI: 10.1080/15376494.2022.2059600.

View | Web of Science ® | Google Scholar

36. A. Tabak, B. Safaei, A. Memarzadeh, S. Arman, and C. Kizilors , An extensive review of piezoelectric energy-harvesting structures utilizing auxetic materials, J. Vib. Eng. Technol., 2023.DOI: https://doi.org/10.1007/s42417-023-01038-9.

View | Web of Science ® | Google Scholar

37. F. Rizzi, S. Puce, F. La Malfa, M. Totaro, M. De Vittorio, and L. Beccai, Modeling and development of an auxetic foam-based multimodal capacitive strain gauge, Smart Mater. Struct., vol. 32, no. 2, pp. 025013, 2023. DOI: 10.1088/1361-665X/acafb7.

View | Web of Science ® | Google Scholar

38. A. Moayedizadeh and D. Younesian, Application of the meta-substrates for power amplification in rotary

DOI: 10.1016/j.egyr.2022.04.022.

View | Web of Science ® | Google Scholar

39. Q.Q. Li, Z.C. He, and E. Li, Dissipative multi-resonator acoustic metamaterials for impact force mitigation and collision energy absorption, Acta Mech., vol. 230, no. 8, pp. 2905–2935, 2019. DOI: 10.1007/s00707-019-02437-4.

View | Web of Science ® | Google Scholar

40. T. Li, F. Liu, and L. Wang, Enhancing indentation and impact resistance in auxetic composite materials, Compos. Part B Eng., vol. 198, pp. 108229, 2020. DOI: 10.1016/j.compositesb.2020.108229.

View | Web of Science ® | Google Scholar

41. M.-F. Guo, H. Yang, and L. Ma, 3D lightweight double arrow-head plate-lattice auxetic structures with enhanced stiffness and energy absorption performance, Compos. Struct., vol. 290, pp. 115484, 2022. DOI: 10.1016/j.compstruct.2022.115484.

View | Web of Science ® | Google Scholar

42. H. Ding, H. Guo, P. Sun, S. Huang, T. Yuan, and Y. Wang, In-plane dynamic crushing of a novel hybrid auxetic honeycomb with enhanced energy absorption, Mech. Adv. Mater. Struct., pp. 1–19, 2023. DOI: 10.1080/15376494.2023.2204082.

View | Web of Science ® | Google Scholar

43. A. Hosseinkhani, D. Younesian, M. Ranjbar, and F. Scarpa, Enhancement of the vibro-acoustic performance of anti-tetra-chiral auxetic sandwich panels using topologically optimized local resonators, Appl. Acoust., vol. 177, pp. 107930, 2021. DOI: 10.1016/j.apacoust.2021.107930.

View | Web of Science ® | Google Scholar

44. S.L. Zhang, Y.-C. Lai, X. He, R. Liu, Y. Zi, and Z. L. Wang, Auxetic foam-based contact-mode triboelectric nanogenerator with highly sensitive self-powered strain sensing capabilities to monitor human body movement, Adv. Funct. Mater., vol. 27, no. 25, pp. 1606695, 2017. DOI: 10.1002/adfm.201606695.

View | Web of Science ® | Google Scholar

45. P. Eghbali, D. Younesian, A. Moayedizadeh, and M. Ranjbar, Study in circular auxetic structures for efficiency enhancement in piezoelectric vibration energy harvesting, Sci. Rep., vol. 10, no. 1, Article no. 16338, 2020. DOI: 10.1038/s41598-020-73425-1.

View | PubMed | Web of Science ® | Google Scholar

46. X. Zhu, J. Zhang, W. Zhang, and J. Chen, Vibration frequencies and energies of an auxetic honeycomb sandwich plate, Mech. Adv. Mater. Struct., vol. 26, no. 23, pp. 1951–1957, 2019. DOI: 10.1080/15376494.2018.1455933.

View | Web of Science ® | Google Scholar

47. S. Sadikbasha, B. Radhika, and V. Pandurangan, Auxetic hexachiral cantilever beams for piezoelectric vibration energy harvesting, Smart Mater. Struct., vol. 31, no. 10, pp. 105015, 2022. DOI: 10.1088/1361-665X/ac8d3e.

View | Web of Science ® | Google Scholar

48. K. Chen, Q. Gao, S. Fang, D. Zou, Z. Yang, and W.-H. Liao, An auxetic nonlinear piezoelectric energy harvester for enhancing efficiency and bandwidth, Appl. Energy, vol. 298, pp. 117274, 2021. DOI: 10.1016/j.apenergy.2021.117274.

View | Web of Science ® | Google Scholar

49. W.J.G. Ferguson, Y. Kuang, K.E. Evans, C.W. Smith, and M. Zhu, Auxetic structure for increased power output of strain vibration energy harvester, Sens. Actuat. A Phys., vol. 282, pp. 90–96, 2018. DOI: 10.1016/j.sna.2018.09.019.

View | Web of Science ® | Google Scholar

50. K. Chen, S. Fang, Z. Lai, J. Cao, and W.-H. Liao, A frequency upconversion rotational energy harvester with auxetic structures for high power output, Smart Mater. Struct., vol. 32, 045019, 2023. DOI: 10.1088/1361-665X/acc220.

View | Google Scholar

51. K. Chadha, V. Mahesh, A.S. Mangalasseri, and V. Mahesh, On analysing vibration energy harvester with auxetic core and magneto-electro-elastic facings, Thin-Walled Struct., vol. 184, pp. 110533, 2023. DOI: 10.1016/j.tws.2023.110533.

View | Web of Science ® | Google Scholar

52. M.H. Fatahi, M. Hamedi, and M. Safarabadi, Experimental and numerical implementation of auxetic substrate for enhancing voltage of piezoelectric sandwich beam harvester, Mech. Adv. Mater. Struct., vol. 29, no. 27, pp. 6107–6117, 2022. DOI: 10.1080/15376494.2021.1972371.

View | Web of Science ® | Google Scholar

53. A. Pagani, M. Boscolo, J.R. Banerjee, and E. Carrera, Exact dynamic stiffness elements based on one-dimensional higher-order theories for free vibration analysis of solid and thin-walled structures, J. Sound Vib., vol. 332, no. 23, pp. 6104–6127, 2013. DOI: 10.1016/j.jsv.2013.06.023.

View | Web of Science ® | Google Scholar

54. R. Augello, E. Daneshkhah, X. Xu, and E. Carrera, Efficient CUF-based method for the vibrations of thin-walled open cross-section beams under compression, J. Sound Vib., vol. 510, pp. 116232, 2021. DOI: 10.1016/j.jsv.2021.116232.

View | Web of Science ® | Google Scholar

55. E. Carrera and V.V. Zozulya, Carrera unified formulation (CUF) for the shells of revolution. Numerical evaluation,

View | Web of Science ® | Google Scholar

56. M. Filippi, R. Azzara, and E. Carrera, Rotordynamic analyses with variable-kinematic beam and shell finite elements, Mech. Adv. Mater. Struct., pp. 1–13, 2023. DOI: 10.1080/15376494.2023.2246221.

View | Web of Science ® | Google Scholar

57. C. He, J. Zhu, Y. Hua, D. Xin, and H. Hua, A study on the vibration characteristics of functionally graded cylindrical beam in a thermal environment using the Carrera unified formulation, Mech. Adv. Mater. Struct., pp. 1–13, 2023. DOI: 10.1080/15376494.2023.2242861.

View | Web of Science ® | Google Scholar

58. J. Shen, M.R. Arruda, A. Pagani, and E. Carrera, A regularized higher-order beam elements for damage analysis of reinforced concrete beams, Mech. Adv. Mater. Struct., pp. 1–13, 2023. DOI: 10.1080/15376494.2023.2245825.

View | Web of Science ® | Google Scholar

59. A. Erturk and D.J. Inman, Piezoelectric Energy Harvesting, John Wiley & Sons, Chichester, United Kingdom, 2011.

View | Google Scholar

60. Q. Li, Y. Kuang, and M. Zhu, Auxetic piezoelectric energy harvesters for increased electric power output, AIP Adv., vol. 7, no. 1, Article no. 015104, 2017. DOI: 10.1063/1.4974310.

View | Web of Science ® | Google Scholar

61. Y. Jiang and Y. Li, 3D printed chiral cellular solids with amplified auxetic effects due to elevated internal rotation, Adv. Eng. Mater., vol. 19, no. 2, pp. 1600609, 2017. DOI: 10.1002/adem.201600609.

Web of Science ® | Google Scholar

62. A. Alomarah, D. Ruan, S. Masood, I. Sbarski, and B. Faisal, An investigation of in-plane tensile properties of re-entrant chiral auxetic structure, Int. J. Adv. Manuf. Technol., vol. 96, no. 5-8, pp. 2013–2029, 2018. DOI: 10.1007/s00170-018-1605-x.

Web of Science ® | Google Scholar

63. P. Eghbali, D. Younesian, and S. Farhangdoust, Enhancement of piezoelectric vibration energy harvesting with auxetic boosters, Int. J. Energy Res., vol. 44, no. 2, pp. 1179–1190, 2020. DOI: 10.1002/er.5010.

Web of Science ® | Google Scholar

64. COMSOL Multiphysics®, v. 5.6. COMSOL AB, Stockholm, Sweden. Available from: www.comsol.com.

Google Scholar

65. J.H. Wu, J. Wang, E. Carrera, and R. Augello, An analysis of the propagation of surface acoustic waves in a

2023. DOI: 10.1080/15376494.2023.2207270.